AIR POLLUTION

Temperature-dependent emissions dominate aerosol and ozone formation in Los Angeles

Eva Y. Pfannerstill[1]*†, Caleb Arata[1], Qindan Zhu[2,3,4]‡, Benjamin C. Schulze[4], Ryan Ward[4], Roy Woods[5], Colin Harkins[3,6], Rebecca H. Schwantes[6], John H. Seinfeld[4], Anthony Bucholtz[5], Ronald C. Cohen[2,7], Allen H. Goldstein[1,8]*

Despite declines in transportation emissions, urban North America and Europe still face unhealthy air pollution levels. This has challenged conventional understanding of the sources of their volatile organic compound (VOC) precursors. Using airborne flux measurements to map emissions of a wide range of VOCs, we demonstrate that biogenic terpenoid emissions contribute ~60% of emitted VOC OH reactivity, ozone, and secondary organic aerosol formation potential in summertime Los Angeles and that this contribution strongly increases with temperature. This implies that control of nitrogen oxides is key to reducing ozone formation in Los Angeles. We also show some anthropogenic VOC emissions increase with temperature, which is an effect not represented in current inventories. Air pollution mitigation efforts must consider that climate warming will strongly change emission amounts and composition.

Ambient air pollution is the fourth-ranking human health risk factor globally (*1*), leading to an estimated 4.2 million premature deaths per year (*2*). Important pollutants causing cardiovascular and respiratory diseases are fine particulate matter ($PM_{2.5}$) and tropospheric ozone (*2*). Volatile organic compounds (VOCs) are precursors to both: A large fraction of $PM_{2.5}$ is secondary organic aerosol (SOA) that forms through the oxidation of VOCs (*3*). In the presence of nitrogen oxides (NO_x) and sunlight, VOC oxidation leads to ozone formation.

Ninety-nine percent of the world's population lives in places where the World Health Organization air quality guidelines are not met (*2*). This includes the US megacity of Los Angeles, where ozone and $PM_{2.5}$ are frequently at unhealthy levels, especially in the summer (*4*, *5*). As in many industrialized cities, technologies such as efficient three-way catalytic converters and efforts spurred by regulation led to a steep decrease in automotive VOC emissions and thus to a decades-long decrease of air pollutant concentrations (*6*). However, concentrations of ozone and $PM_{2.5}$ particle pollution have stopped decreasing since ~2010 (*7*, *8*). Recent studies indicate the increasing relative importance of volatile chemical products, which now contribute as much as half of urban fossil fuel VOC emissions in industrialized cities (*9*, *10*). The relative contribution of the biogenic VOC fraction must also have increased with declining transportation emissions. As a result of these changes in the emitted VOC mixture over the course of a few decades, the sources of secondary air pollution have been called into question. For example, model-observation comparisons have raised doubts on whether the models correctly reproduce the emission source mixture contributing to SOA (*11*, *12*). The origin of SOA in Los Angeles is under debate, with some studies reporting a predominantly vehicular source (*11*, *13*), whereas a temperature-dependent analysis of $PM_{2.5}$ concentrations and isoprene concentrations indicated a major biogenic origin (*8*). The percentage of days on which $PM_{2.5}$ exceeds 12 $\mu g/m^3$ is <10% at 20°C and >40% at 30°C and reaches 70% at 40°C (*8*). Similarly, the likelihood of ozone exceedances (≥70 parts per billion) is close to 0% at 20°C and >70% at temperatures ≥30°C, with temperature-dependent biogenic emissions of reactive terpenoids suggested as one of the driving factors (*14*). However, concentration-based temperature dependencies may be influenced by meteorology instead of emissions because hotter days tend to be more stagnant (*15*). This shows the need for direct emission observations. With climate change, an increase in the number of days with high temperatures is expected (*16*, *17*). Thus, it is important to understand how increasing temperatures affect VOC emission amounts and mixture and what this means for secondary air pollutant formation, as well as regulation strategies.

[1]Department of Environmental Science, Policy and Management, University of California at Berkeley, Berkeley, CA, USA. [2]Department of Earth and Planetary Science, University of California at Berkeley, Berkeley, CA, USA. [3]Cooperative Institute for Research in Environmental Sciences, University of Colorado Boulder, Boulder, CO, USA. [4]NOAA Chemical Sciences Laboratory, Boulder, CO, USA. [5]Department of Environmental Science and Engineering, California Institute of Technology, Pasadena, CA, USA. [6]Department of Meteorology, Naval Postgraduate School, Monterey, CA, USA. [7]Department of Chemistry, University of California at Berkeley, Berkeley, CA, USA. [8]Department of Civil and Environmental Engineering, University of California at Berkeley, Berkeley, CA, USA.
*Corresponding author. Email: ahg@berkeley.edu (A.H.G.); e.pfannerstill@fz-juelich.de (E.Y.P.)
†Present address: Institute for Energy and Climate Research 8: Troposphere, Forschungszentrum Jülich, Jülich, Germany.
‡Present address: Department of Earth, Atmospheric and Planetary Sciences, Massachusetts Institute of Technology, Cambridge, MA, USA.

Spatially resolved direct airborne measurements of VOC emission fluxes

Previous efforts to understand the magnitude and composition of VOC emissions in Los Angeles, as in other megacities, have relied on indirect methods—either by using traditional bottom-up emission inventories (*18*) or by inferring emissions top down from concentration measurements with chemical transport models (*10*). Both approaches are indirect and rely on a range of assumptions and thus are subject to large uncertainties. To overcome these limitations, we performed airborne eddy covariance measurements to provide the first direct observations of spatially resolved VOC emissions in Los Angeles. Emission and deposition fluxes were calculated from 10-Hz concentration and vertical wind speed measurements by using continuous wavelet transformation (*19*). State-of-the-art instrumentation [proton transfer reaction (PTR)–time-of-flight mass spectrometry–time-of-flight mass spectrometry] provided a comprehensive range of VOC species for which spatially resolved urban fluxes were observed, including source-specific tracers for biogenics, vehicle emissions, personal care products, and solvents, among others. Nine flights were conducted in June 2021 between 11:00 and 17:00, with flight days selected to cover a temperature range as wide as possible (for maps of flight tracks, see figs. S1 and S5). Median flight temperatures ranged from 23° to 31°C, with minima and maxima stretching from 15° to 37°C, respectively.

Ozone formation in Los Angeles is still sensitive to VOCs, with recent analyses suggesting that current NO_x emissions need to be reduced substantially (>50%) to move to a NO_x-sensitive ozone formation regime (*7*, *14*). The contribution of VOCs to ozone formation depends on the reaction frequency of each VOC species with the hydroxyl (OH) radical, the primary oxidant in the daytime troposphere. This reaction frequency is referred to as VOC OH reactivity (hereafter: OH reactivity) and is calculated for emissions as

$$\mathrm{OHR}_F = k_{\mathrm{OH,VOC}} \times F_{\mathrm{VOC}} \quad (1)$$

where OHR_F is the OH reactivity of the flux in meters per second squared, $k_{\mathrm{OH,VOC}}$ is the reaction rate constant of a VOC with the OH radical in meter cubed per molecule per second, and F_{VOC} is the flux of the VOC in molecules per meter squared per second. Because the daytime boundary layer over Los Angeles can be considered as a box to which emissions are continuously added, emitted OH reactivity can be considered a proxy for in situ ozone formation potential within the Los Angeles basin. The contribution of VOCs to SOA formation is more complex to quantify. We estimated aerosol yields using the statistical oxidation model (*20*) combined with a one-dimensional volatility

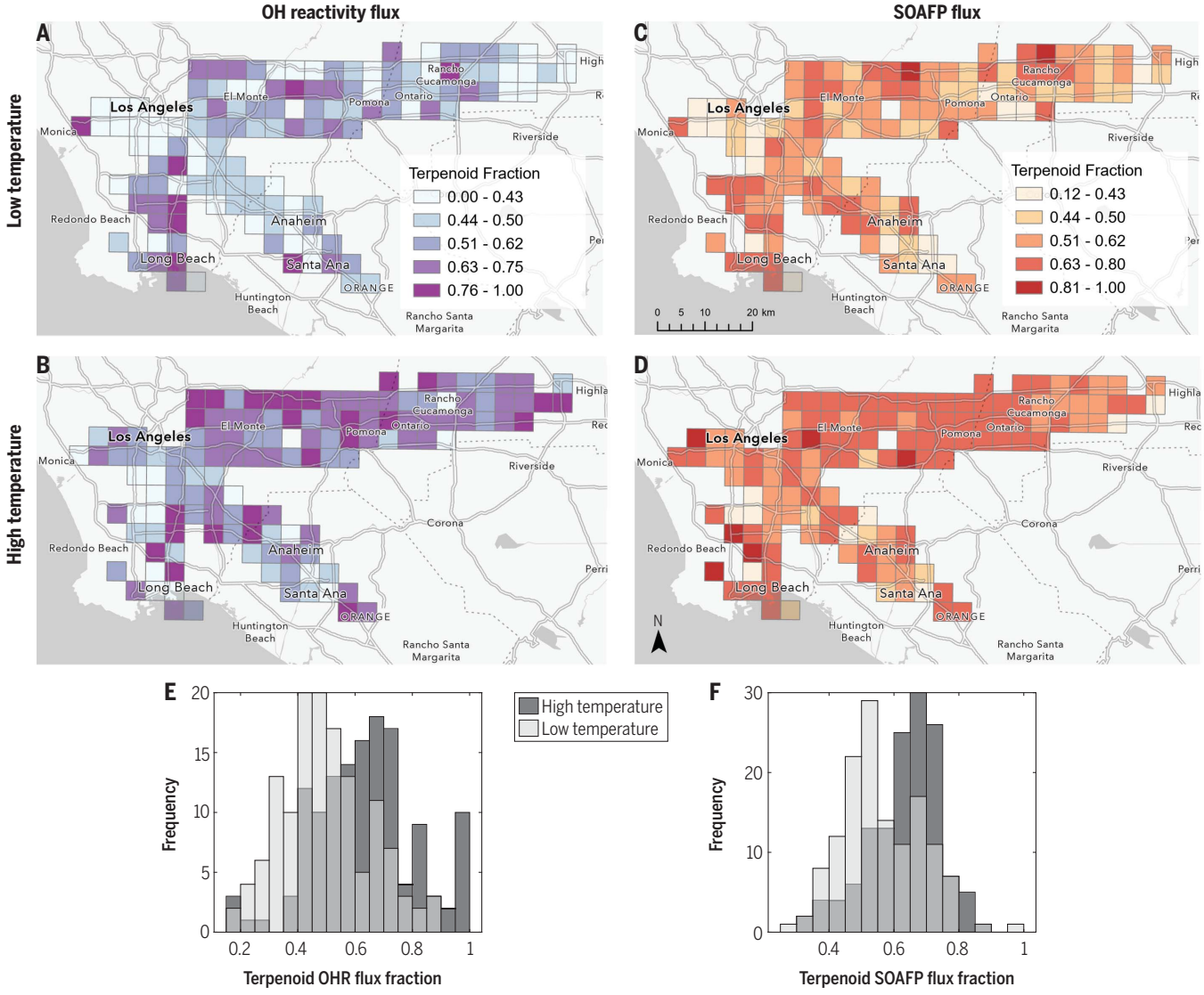

Fig. 1. Terpenoid fraction of OH reactivity and SOA formation potential of measured emissions at low versus high temperatures in Los Angeles. (**A** to **D**) Maps show the terpenoid [isoprene (C_5H_8) + monoterpenes ($C_{10}H_{16}$, $C_{10}H_{16}O$, $C_{10}H_{18}O$) + sesquiterpenes ($C_{15}H_{24}$)] fraction in the summed VOC OH reactivity flux at low temperature (A), high temperature (B), and in the summed SOA formation potential (SOAFP) of VOC emissions at low (C) and high (D) temperatures. For each 4-km by 4-km grid cell, "low temperature" was defined as an ambient temperature (2 m above ground) in the lowest 25% of all flux measurements ($n \geq 6$) conducted over that grid cell, and "high temperature" was defined as an ambient temperature in the upper 25% of all flux measurements conducted over that grid cell. (**E** and **F**) Frequency of grid cells' terpenoid fractions at low (E) and high (F) temperatures is shown. OHR, OH reactivity of the flux; SOAP, SOA potential.

basis set for oxygenated VOCs (*21*). Ambient particle formation also depends on factors such as ambient humidity (*22*), preexisting particle surface area (*23*), and the mixture of VOCs present (*24*), which we have not considered here but are unlikely to substantially change the relative contribution of individual precursor classes to the SOA budget.

Temperature dependence of the VOC mixture contributing to secondary air pollutants

Mapped VOC emissions (fig. S5) were attributed to footprint areas (fig. S1) and averaged to 4-km by 4-km grid cells, and the VOC OH reactivity and SOA formation potential were calculated for each of the observed 410 VOC species. The fraction of terpenoids (isoprene, monoterpenes, and sesquiterpenes, typically attributed to biogenic emissions) both in the summed OH reactivity and SOA formation potential was large even in the lowest temperature bin and grew substantially with temperature in most areas of Los Angeles (Fig. 1). In the lower 25th percentile of temperatures, OH reactivity in 45% of the grid cells and SOA formation potential in 67% of the grid cells were dominated by terpenoids. This especially included regions at the less urbanized hillsides on the outskirts of the metropolitan area, for example, north of El Monte. In the top 25th percentile, these values increased to 78 and 88%, respectively. Thus, at high temperatures, terpenoids became the main drivers for the formation potential of ozone and particles even in the downtown area (in Fig. 1 below and southeast of the label "Los Angeles"), where traffic and consumer product emissions are expected to be largest on the basis of current emission inventories.

The composition of the observed average VOC emission mixture is shown in Fig. 2 (for high and low temperature composition, see fig. S6). Terpenoids contributed ~16% of the measured VOC mass flux. Owing to the high reactivity of the terpenoids and the low volatility of their oxidation products, terpenoids accounted for 56 ± 26% of the emitted OH reactivity and 56 ± 33% of the SOA formation potential. The OH reactivity contribution here

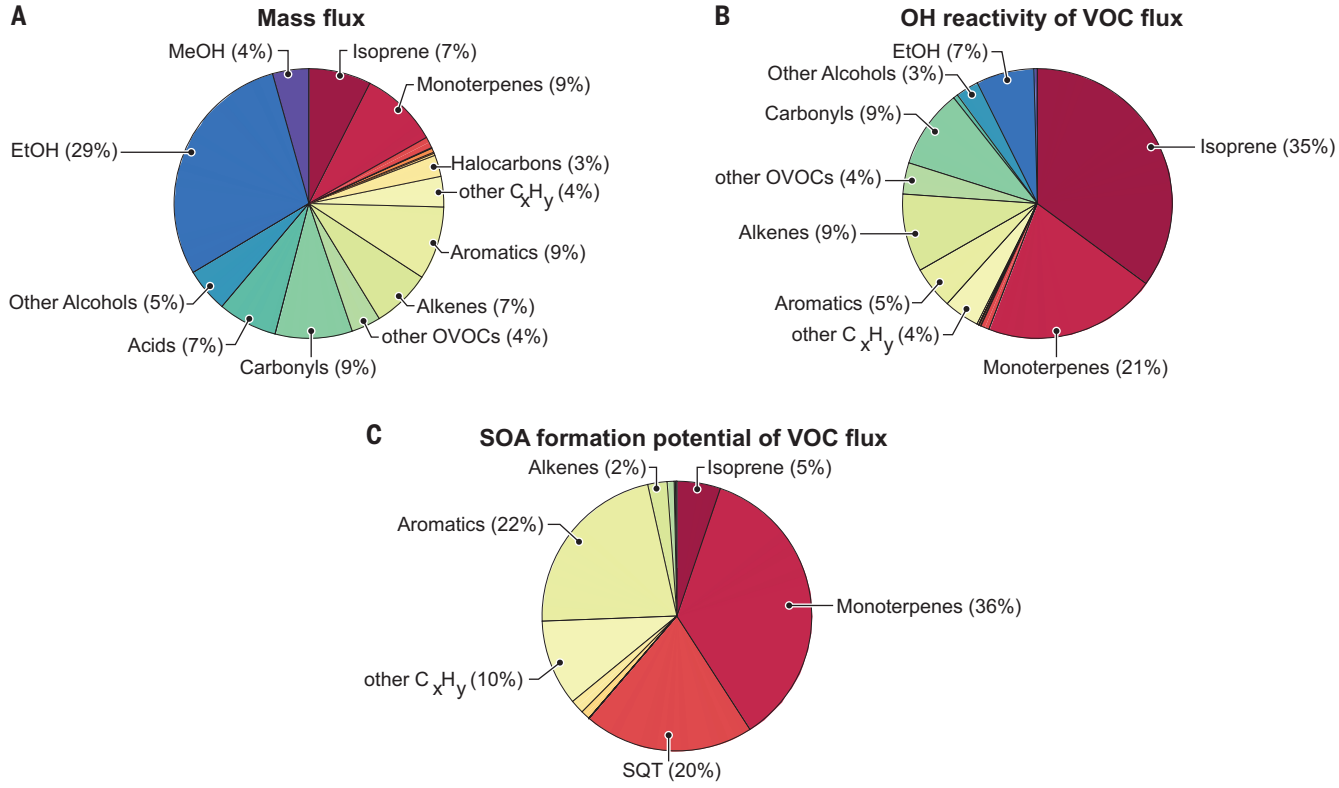

Fig. 2. Contribution of different VOC classes. (**A** to **C**) Contributions of VOC classes to (A) mass flux, (B) OH reactivity of VOC flux, and (C) SOAFP of VOC surface flux of all VOCs measured during the RECAP-CA flights in June 2021. Alkanes (contributing up to 4% of emitted OH reactivity and up to 24% of SOAFP) were not measured. The pie charts show the median composition over all flights. EtOH, ethanol; MeOH, methanol; OVOC, oxygenated VOC; SQT, sesquiterpenes.

is similar to the ~60% biogenic contribution to ozone in Berlin during a heatwave (*25*) and is supported by a modeling analysis for Los Angeles that showed that terpenoids and NO_x combined contribute >55% of the MDA8 ozone formed in Los Angeles (*26*). An inventory-based study also found ~50% contribution of biogenic terpenoids to ozone formation potential in Los Angeles, although with a higher isoprene and a lower monoterpene contribution (*18*). The same study predicted only 23% of the (annual average) SOA formation potential from terpenoids, but our value agrees well with a radiocarbon analysis of organic aerosol in summertime Los Angeles that attributed 58% ± 15% to nonfossil sources (*27*). Ethanol, which was a major constituent of the VOC mass flux, is a low-reactivity VOC and thus only contributed ~5% of the OH reactivity. The terpenoid fraction here is higher than in concentration-based Los Angeles observations (*28*). Because these VOCs react rapidly, the magnitude of their contribution to secondary products may be underestimated on the basis of ambient concentrations alone.

We note that the VOC emission mixture observed here is incomplete, because the PTR method is not sensitive to alkanes. However, alkanes are a comparably minor and relatively unreactive fraction of total VOC, contributing only 4% of the measured mid-day VOC OH reactivity in Los Angeles in 2010 (*28*). Alkanes, which are longer-lived than terpenoids, would become more relevant contributors to ozone formed downwind of the Los Angeles basin. For SOA formation, long-chain alkanes are of higher relevance. We estimate that including long-chain alkanes would reduce the relative terpenoid contribution to average summertime SOA formation by 24% of the total (*18*). Seasonality and diel variability in emissions composition are not captured by our measurements, which are limited to daytime in June, a time period that is, however, representative for air quality standard exceedance conditions.

The VOCs included in Fig. 3 were among the largest contributors to OH reactivity and/or SOA formation potential of the emissions, and they all increased with temperature. The observed increase of isoprene, monoterpene and sesquiterpene emissions with temperature is in accordance with the expectations for biogenic emissions (*29*). Reflecting this state of knowledge, two current inventories (CARB/MEGAN and the combination of BEIS + FIVE-VCP) also predicted increases in emissions of these VOCs with temperature. However, the measured amount of monoterpene and sesquiterpene emissions was a factor of 2 to 3 higher than predicted by the inventories, and Fig. 3B indicates that temperature sensitivity of monoterpene emissions in the inventories may be underestimated, as shown in a recent evaluation of the MEGAN model (*30*). The measured isoprene emission matched the inventories within the uncertainty of the fluxes.

The observed emissions of several anthropogenic VOCs also increased with temperature. These include toluene (Fig. 3D), ethanol (Fig. 3E), and para-chlorobenzotrifluoride (PCBTF) (Fig. 3F). The observed temperature dependences of ethanol and toluene emissions in the temperature range of 20° to 30°C approximately agree with their vapor pressure curves in this temperature range (*31*). Toluene, ethanol, and PCBTF can come from solvent-based sources, for which evaporative volatilization could explain the temperature dependence. Moreover, evaporative losses from gasoline can become an important contributor to vehicle emissions at high temperatures (*32*). The temperature dependence of these anthropogenic VOCs was not represented in either of the two inventories.

As a result of the increase of VOC emissions with temperature, the summed OH reactivity of the emissions increased two- to threefold from 20° to 30°C (Fig. 4A). This amounts to a 27% increase per 1°C (fig. S8). Although there was an increase in both the emissions of terpenoids and all other VOCs, most of the overall increase was due to the terpenoid emissions alone, which increased more than threefold. The OH reactivity of non-terpenoid VOC emissions only doubled in the

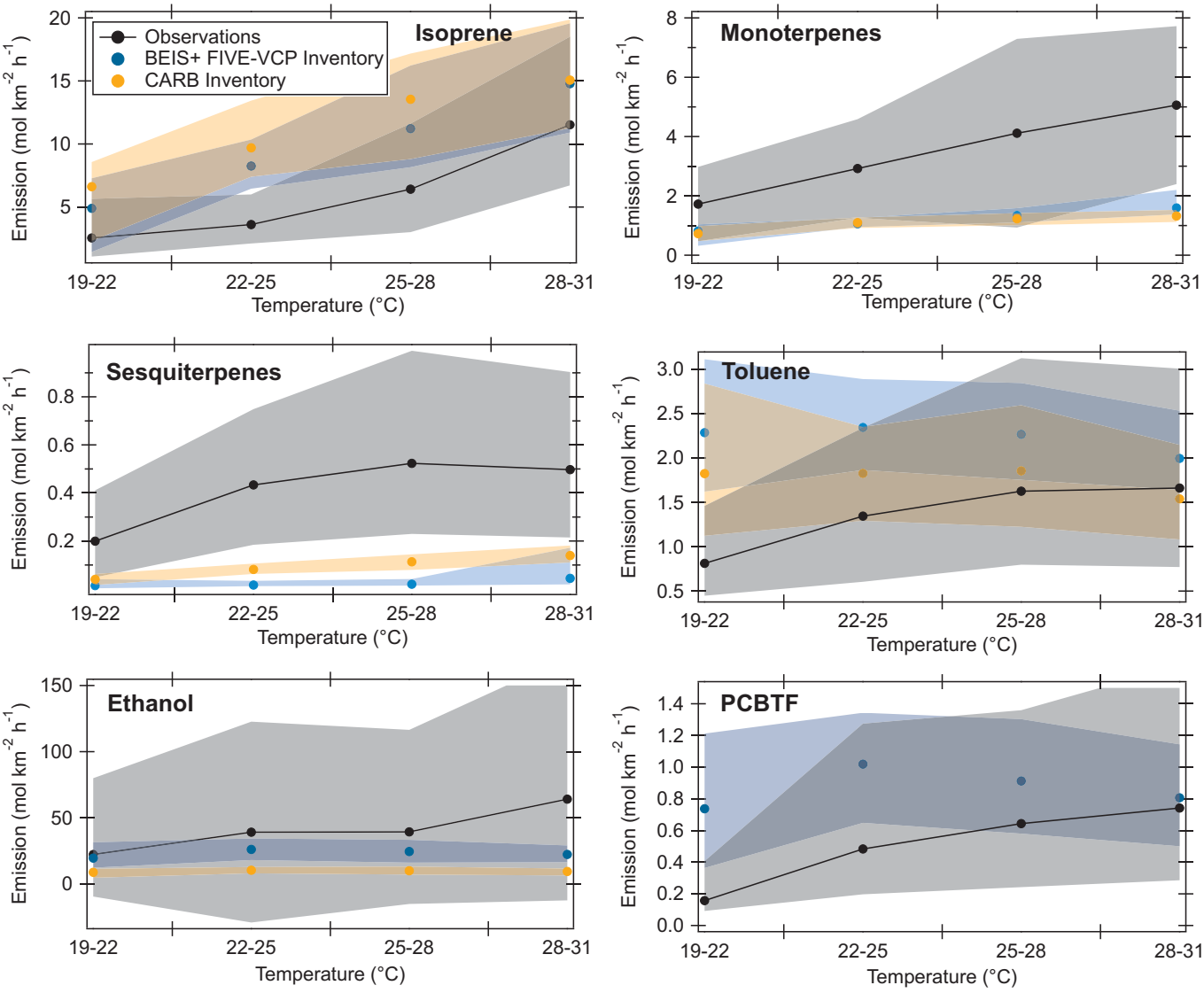

Fig. 3. Temperature dependence of emissions of individual VOC species in comparison with inventories. The VOC species shown here are among the largest contributors to SOAFP and OH reactivity in the measured VOC emissions. The circles represent medians of each temperature bin, and the shaded areas the 25th to 75th percentile of data. The temperature effect cannot be explained with regional emission differences that may co-occur with temperature differences (fig. S7). Measurement uncertainties are 76 to 96%. PCBTF is not included in the CARB inventory. Only temperature bins that include data from all regions (fig. S1) are shown. For flux measurement maps of these six species, see fig. S5.

same temperature range. The terpenoid fraction in the sum of the OH reactivity of VOC emissions increased from ~40% at 20°C to ~60% at 30°C.

Similar to OH reactivity, the SOA formation potential of emitted VOCs increased two- to threefold from 20° to 30°C, or 13% per 1°C temperature increase (Fig. 4B and fig. S8). The terpenoid fraction was enhanced from 45 to 64% of the overall SOA formation from 20° to 30°C, with the SOA-relevant terpenoid emissions approximately doubling in the same temperature range. The SOA-relevant nonterpenoid VOCs—mainly aromatics (Fig. 2)—barely increased with temperature (Fig. 4B). Although the emissions of the aromatic toluene were temperature dependent (Fig. 3) because it has a large solvent source, many other aromatics are mainly tailpipe emissions, which do not change with ambient temperature.

Monoterpene sources: Biogenic or anthropogenic?

Because monoterpenes are an especially relevant contributor to SOA formation and OH reactivity in Los Angeles, understanding whether their source is anthropogenic or biogenic is critical for air quality management. Recently, anthropogenic sources of urban monoterpenes, especially D-limonene, have been reported (*33*). Monoterpenes and sesquiterpenes are present in a variety of fragranced consumer products, for example, cleaning or personal care products (*34*).

Our data suggest a dominant, but not sole, biogenic source for the monoterpenes. The biogenic dominance is indicated both by the temperature dependence (Fig. 3B) (*35*) and by the correlation between monoterpenes and biogenic isoprene in fluxes measured in the downtown Los Angeles region (Fig. 5A). In the same region, we did not observe correlations between monoterpenes and any of the identified anthropogenic tracers, such as D5 siloxane (personal care product tracer) (Fig. 5B), toluene, or ethanol (fig. S9). Because the sesquiterpene fluxes correlated well with the monoterpene fluxes (fig. S9), a dominant biogenic source for the sesquiterpenes can be assumed, too. Monoterpene emissions did not scale with inventories of tree and shrub cover (figs. S10 and S11), likely

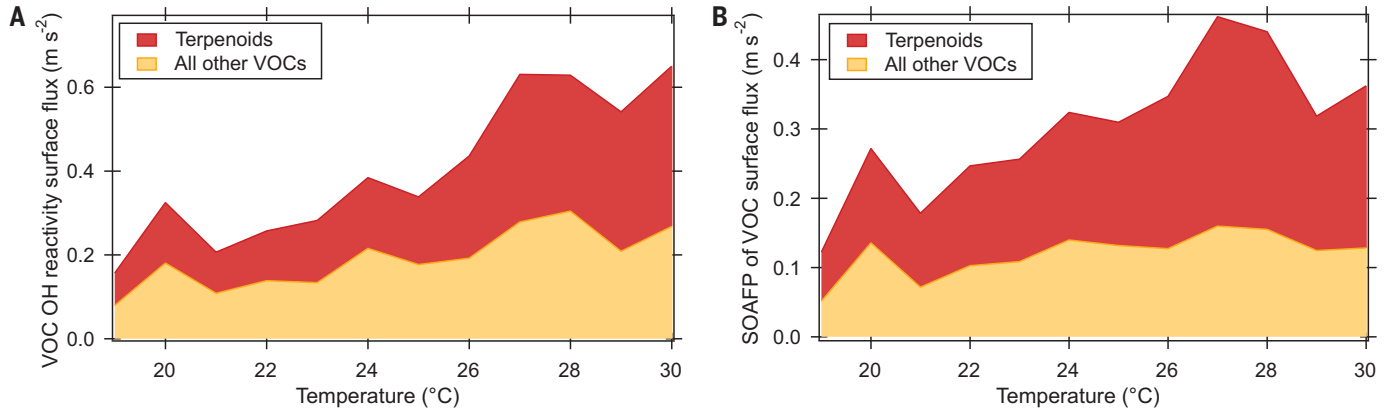

Fig. 4. Temperature dependence of the summed OH reactivity and SOAFP of the VOC emissions. (**A**) OH reactivity and (**B**) SOAFP of emitted VOCs. Primary terpenoid contribution was separated from all other VOCs and is shown as the red fraction of the stacked plot. All measured fluxes were binned into 1°C temperature bins for this plot, where "temperature" is the ambient temperature at 2 m above ground level. To ensure that the dependence is not skewed by regional emission differences, only temperature bins that cover at least three regions were included. Alkanes (contributing up to 4% of emitted OH reactivity and up to 24% of SOAFP) were not measured.

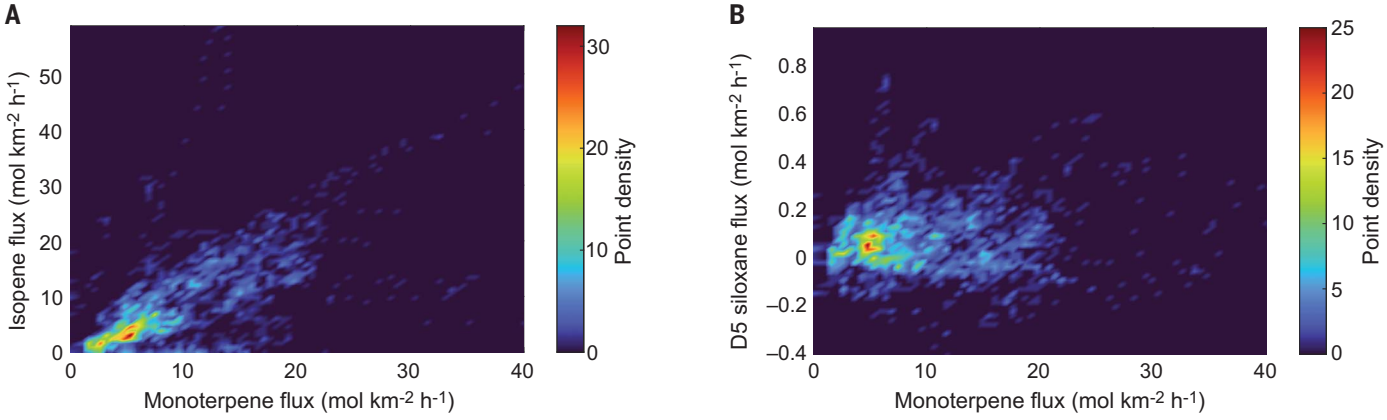

Fig. 5. Correlation of monoterpene emissions in downtown Los Angeles with other VOC fluxes, indicating biogenic origin of monoterpenes. (**A**) Density plot showing correlation (r = 0.7) between monoterpene fluxes and isoprene fluxes in the Los Angeles downtown region (for definition of regions, see fig. S1). (**B**) No correlation (r = 0.25) of monoterpene fluxes with the fluxes of an anthropogenic tracer, D5 siloxane, in the downtown Los Angeles region.

because not all trees or shrubs are monoterpene emitters. Biogenic emission inventories such as the ones included in our comparison (Fig. 3B) do not consider plant species variability within urban areas and therefore do not represent potential spatial differences in the composition and emission factors of biogenic emissions per tree. We observed regional differences in the isoprene/monoterpene emission ratio, which was ~3 in San Bernardino and ~1.5 in downtown, even though both regions have similar fractional tree coverage (fig. S12). Likely, the species composition in the San Bernardino Valley with its hillside shrublands is different.

Nonetheless, there are indications for an anthropogenic influence on measured monoterpene emissions: Some high monoterpene emissions in downtown Los Angeles (Fig. 5A) were not correlated with isoprene. In New York in winter, that is, when plant emissions are assumed to be low, monoterpenes scaled with population density (*33*). However, in Los Angeles in summer, we did not observe a correlation between monoterpene emissions and population density in the flux footprint. (This differs from the personal care product tracer D5 siloxane, which did correlate with population density; see fig. S10.) Because of this observation, we infer that a dominant anthropogenic monoterpene source is unlikely. A nonnegative matrix factorization of monoterpene and other VOC fluxes with tree cover, temperature, and population density assigned ~33% of the variability in monoterpenes fluxes to a factor dominated by population density, whereas the rest of the variability was explained by temperature and by tree and shrub cover (fig. S13). This is in good agreement with a source-apportionment study in Atlanta, Georgia, that attributed 26% of the monoterpenes to anthropogenic sources (*35*) and in which anthropogenic monoterpenes did not correlate with temperature. Coggon *et al*. suggested an anthropogenic source of monoterpenes in New York of up to 860 mg person^{-1} day^{-1} (*10*), which, by applying the population density in our flux footprints, would amount to a median of 0.74 mol km^{-2} hour^{-1} or 15% of observed monoterpenes emitted in Los Angeles.

The observed monoterpene and sesquiterpene emissions were significantly higher than predicted by the CARB and BEIS + FIVE-VCP inventories (Fig. 3). Although this may indicate an anthropogenic source not incorporated in the inventories, the size of the mismatch suggests another missing source. Because the inventories only consider an average urban tree composition, specific local monoterpene emitters may be missing, for example, eucalyptus trees, which comprise 5% of Los Angeles tree population. Moreover, flowering emissions are not included in the inventories. For example, jacaranda (*Jacaranda* sp.) trees, which are among the most abundant species in Los Angeles (*36*), were in bloom during the aircraft observations. Monoterpene emissions during bloom can be up to an order of magnitude higher than usual (*37*, *38*), and jacaranda flowers have been shown to emit a bouquet that includes monoterpenes and is rich in sesquiterpenes

(*39*, *40*). Another factor that can substantially increase biogenic terpenoid emissions and is not part of inventories is heat or drought stress (*41*, *42*). Long-term drought stress has been shown to increase sesquiterpene and monoterpene emissions while reducing isoprene emissions (*42*, *43*), which agrees with our observed inventory discrepancies. In California, 2021 was one of the driest and hottest years on record (*44*). Another contributing factor for the mismatch between observations and inventory may be the uncertainty of biogenic emission factors, their temperature dependence, and their parameterization (*30*, *45*).

Implications for urban air quality in a warming climate

Climate change is predicted to increase the number of hot days, with disproportionately large temperature increases in urban areas and in the summer (*16*, *17*). Average summer temperatures in the Los Angeles region are projected to increase by 3°C by the 2060s (*17*). Our results imply that this would lead to a doubling in emitted OH reactivity and a 40% increase in SOA formation potential of the VOCs represented in this work. This calculation assumes a linear increase in emitted OH reactivity and SOA formation potential with temperature, as observed in the limited temperature range covered in our study. Monoterpene and sesquiterpene emissions typically increase exponentially with temperature, whereas isoprene emissions are known to increase with temperature and light and eventually decrease above a temperature threshold (*46*). The biogenic VOC emission response to long-term climate change effects is subject to many uncertainties, although most studies report increased terpenoid emissions in response to warming (*47*). Our data suggest that terpenoids dominate the SOA formation potential and emitted OH reactivity above 30°C. Historically, only 10% of July days in coastal Southern California exceeded 30°C. By the 2060s, this fraction is predicted to increase to 50% (*17*). In inland Los Angeles regions, even current July temperatures exceed 30°C (*17*) nearly every day, and therefore, biogenic sources likely already dominate SOA and ozone production. This development could partly be counteracted by increased heat and drought stress that can cause irreversible damage to plants (*48*).

Even at lower summer temperatures, biogenic terpenoids dominate secondary pollutant formation potential in many parts of Los Angeles. The inventory underestimation of mono- and sesquiterpene emissions caused a factor of ~2 underestimation of VOC SOA formation potential (fig. S14) and may explain the gap between modeled and measured SOA (*49*). This, combined with the fact that inventories also did not capture the temperature dependence of anthropogenic VOCs, has implications for the representation of the emission mixture in general and for predicting how the composition and pollutant formation changes as temperatures increase.

Our findings underscore that climate change may lead to more high-ozone and high-$PM_{2.5}$ pollution events unless anthropogenic emissions are substantially reduced (*50*–*52*). Flowering and drought stress periods are expected to increase biogenic terpenoid emissions and may therefore be especially prone to high-ozone and particle pollution events. On high-temperature days, it becomes even more important to reduce NO_x emissions and anthropogenic VOC emissions, because biogenic emissions cannot be regulated and anthropogenic SOA is thought to pose a higher health risk by mass than biogenic SOA (*53*). A further reduction in NO_x emissions will help alleviate the ozone burden after transitioning to a NO_x-limited ozone formation regime.

REFERENCES AND NOTES

1. C. J. L. Murray *et al*., *Lancet* **396**, 1223–1249 (2020).
2. World Health Organization, "World Health Statistics 2022, Monitoring health for the SDGs, sustainable development goals" (2022); https://www.who.int/publications/i/item/9789240051157.
3. P. L. Hayes *et al*., *J. Geophys. Res. Atmos.* **118**, 9233–9257 (2013).
4. US Environmental Protection Agency (EPA), "Air Data - Ozone Exceedances" (2016); https://www.epa.gov/outdoor-air-quality-data/air-data-ozone-exceedances.
5. US EPA, "Air Data - Daily Air Quality Tracker" (2020); https://www.epa.gov/outdoor-air-quality-data/air-data-daily-air-quality-tracker.
6. C. Warneke *et al*., *J. Geophys. Res.* **117**, D00V17 (2012).
7. S.-W. Kim, B. C. McDonald, S. Seo, K.-M. Kim, M. Trainer, *J. Geophys. Res. Atmos.* **127**, e2021JD035606 (2022).
8. C. M. Nussbaumer, R. C. Cohen, *Environ. Sci. Technol.* **55**, 3549–3558 (2021).
9. B. C. McDonald *et al*., *Science* **359**, 760–764 (2018).
10. M. M. Coggon *et al*., *Proc. Natl. Acad. Sci. U.S.A.* **118**, e2026653118 (2021).
11. P. L. Hayes *et al*., *Atmos. Chem. Phys.* **15**, 5773–5801 (2015).
12. P. K. Ma *et al*., *Atmos. Chem. Phys.* **17**, 9237–9259 (2017).
13. Y. Zhao, D. S. Tkacik, A. A. May, N. M. Donahue, A. L. Robinson, *Environ. Sci. Technol.* **56**, 15328–15336 (2022).
14. C. M. Nussbaumer, R. C. Cohen, *Environ. Sci. Technol.* **54**, 15652–15659 (2020).
15. D. E. Horton, C. B. Skinner, D. Singh, N. S. Diffenbaugh, *Nat. Clim. Chang.* **4**, 698–703 (2014).
16. G. C. Hulley, B. Dousset, B. H. Kahn, *Earths Futur.* **8**, e2020EF001480 (2020).
17. D. W. Pierce *et al*., *Clim. Dyn.* **40**, 839–856 (2013).
18. S. Gu, A. Guenther, C. Faiola, *Environ. Sci. Technol.* **55**, 12191–12201 (2021).
19. T. Karl *et al*., *J. Atmos. Sci.* **70**, 3277–3287 (2013).
20. A. L. Robinson *et al*., *Science* **315**, 1259–1262 (2007).
21. C. D. Cappa, K. R. Wilson, *Atmos. Chem. Phys.* **12**, 9505–9528 (2012).
22. G. I. Gkatzelis *et al*., *Geophys. Res. Lett.* **48**, e2020GL091351 (2021).
23. N. S. Holmes, *Atmos. Environ.* **41**, 2183–2201 (2007).
24. G. McFiggans *et al*., *Nature* **565**, 587–593 (2019).
25. G. Churkina *et al*., *Environ. Sci. Technol.* **51**, 6120–6130 (2017).
26. Q. Zhu *et al*., *Atmos. Chem. Phys.* **24**, 5265–5286 (2024).
27. P. Zotter *et al*., *J. Geophys. Res. Atmos.* **119**, 6818–6835 (2014).
28. R. F. Hansen *et al*., *J. Geophys. Res. Atmos.* **126**, e2020JD032988 (2021).
29. A. B. Guenther *et al*., *Geosci. Model Dev.* **5**, 1471–1492 (2012).
30. E. Bourtsoukidis *et al*., *Commun. Earth Environ.* **5**, 23 (2024).
31. National Institute of Standards and Technology, *NIST Webbook* (2022); https://webbook.nist.gov/chemistry/form-ser/.
32. J. I. Rubin, A. J. Kean, R. A. Harley, D. B. Millet, A. H. Goldstein, *J. Geophys. Res.* **111**, 2005JD006458 (2006).
33. G. I. Gkatzelis *et al*., *Environ. Sci. Technol.* **55**, 188–199 (2021).
34. A. C. Steinemann *et al*., *Environ. Impact Assess. Rev.* **31**, 328–333 (2011).
35. Y. Peng *et al*., *Atmos. Environ.* **288**, 119324 (2022).
36. E. G. McPherson, Q. Xiao, E. Aguaron, *Landsc. Urban Plan.* **120**, 70–84 (2013).
37. S. Fares *et al*., *Atmos. Environ.* **45**, 4557–4568 (2011).
38. R. Baghi, D. Helmig, A. Guenther, T. Duhl, R. Daly, *Biogeosciences* **9**, 3777–3785 (2012).
39. C. A. S. Pontes *et al*., *Org. Divers. Evol.* **22**, 527–541 (2022).
40. E. Guimarães, L. C. di Stasi, Rde. C. Maimoni-Rodella, *Ann. Bot.* **102**, 699–711 (2008).
41. J. K. Holopainen *et al*., *Front. Plant Sci.* **9**, 1445 (2018).
42. C. Werner *et al*., *Science* **374**, 1514–1518 (2021).
43. M. J. Potosnak *et al*., *Atmos. Environ.* **84**, 314–322 (2014).
44. California Department of Water Resources, "Water Year 2021: An Extreme Year" (2021); https://water.ca.gov/-/media/DWR-Website/Web-Pages/Water-Basics/Drought/Files/Publications-And-Reports/091521-Water-Year-2021-broch_v2.pdf.
45. L. Kaser *et al*., *Atmos. Chem. Phys.* **22**, 5603–5618 (2022).
46. A. B. Guenther, P. R. Zimmerman, P. C. Harley, R. K. Monson, R. Fall, *J. Geophys. Res.* **98**, 12609–12617 (1993).
47. J. Peñuelas, M. Staudt, *Trends Plant Sci.* **15**, 133–144 (2010).
48. E. Kleist *et al*., *Biogeosciences* **9**, 5111–5123 (2012).
49. E. A. Pennington *et al*., *Atmos. Chem. Phys.* **21**, 18247–18261 (2021).
50. D. J. Jacob, D. A. Winner, *Atmos. Environ.* **43**, 51–63 (2009).
51. E. von Schneidemesser *et al*., *Chem. Rev.* **115**, 3856–3897 (2015).
52. S. Wu *et al*., *J. Geophys. Res.* **113** (D6), 2007JD008917 (2008).
53. C. Lovett *et al*., *F1000Res.* **7**, 1031 (2018).
54. E. Y. Pfannerstill, Airborne VOC flux analysis code 2023, Zenodo (2023); https://zenodo.org/records/8411339.
55. Q. Zhu *et al*., qdzhu/FLUX: v1.0 qdzhu/FLUX: First release, Zenodo (2023); https://zenodo.org/records/8425485.

ACKNOWLEDGMENTS

The authors thank D. Baldocchi, G. Wolfe, E. Delaria, and T. Wang for insightful discussions about vertical flux divergence; A. Guenther for providing a tree cover inventory; B. McDonald for help with SOA formation potentials; M. Coggon, C. Stockwell, and C. Warneke for valuable discussions on PTR–time-of-flight mass spectrometry VOC corrections; the Regional Chemical Modeling Group of NOAA CSL for help with weather forecasting; and the Modeling and Meteorology Branch at CARB for providing their inventory. We gratefully acknowledge G. Cooper for excellent mission support; the pilots B. Kujat and G. Loudakis for their dedicated help in flight preparation, planning, and execution; and R. Weber and E. Katz for logistical support. We also thank NOAA's High Performance Computing and Communications program. **Funding:** California Air Resources Board contract nos. 20RD003 and 20AQP012 (to A.H.G. and R.C.C.); NOAA Climate Program Office's Atmospheric Chemistry, Carbon Cycle, and Climate program, grant no. NA22OAR4310540 (UCB)/ NA22OAR4310541 (AD) (to A.H.G.); Office of Naval Research Defense University Research Instrumentation Program grant no. N00014-19-1-2108 (to A.H.G.); Presidential Early Career Award for Scientists and Engineers (PECASE) (to Brian McDonald); Alexander von Humboldt Foundation Feodor Lynen Fellowship (to E.Y.P.); EPA-STAR grant no. 84001001 (to R.H.S. and Q.Z.). The views expressed in this article are those of the authors and do not necessarily represent the views or policies of the US Environmental Protection Agency. The EPA does not endorse any products or commercial services mentioned in this publication. **Author contributions:** Conceptualization: A.H.G. and R.C.C; Methodology: E.Y.P., C.A., Q.Z., and R.H.S.; Software: E.Y.P., C.A., and Q.Z.; Investigation: E.Y.P., C.A., B.C.S., A.B., and R. Wa., and R. Wo. Formal analysis: E.Y.P.; Visualization: E.Y.P.; Funding acquisition: A.H.G., R.C.C., and R.H.S.; Project administration: A.H.G., R.C.C., and A.B.; Supervision: A.H.G. and R.C.C.; Writing – original draft: E.Y.P.; Writing – review and editing: All authors. **Competing interests:** The authors declare that they have no competing interests. **Data and materials availability:** All data used for this manuscript are available at https://csl.noaa.gov/projects/sunvex/. The codes used for wavelet flux analysis and footprint calculation are available online (*54*, *55*).

SUPPLEMENTARY MATERIALS

science.org/doi/10.1126/science.adg8204
Materials and Methods
Figs. S1 to S16
Table S1 and S2
References (*56*–*103*)
Data S1

Submitted 1 March 2023; accepted 22 April 2024
10.1126/science.adg8204